CellPress

Neuron
Article

Structural and Molecular Remodeling of Dendritic Spine Substructures during Long-Term Potentiation

Miquel Bosch,[1,2,*] Jorge Castro,[2,5] Takeo Saneyoshi,[3,5] Hitomi Matsuno,[3] Mriganka Sur,[2] and Yasunori Hayashi[1,2,3,4,*]
[1]RIKEN-MIT Neuroscience Research Center
[2]The Picower Institute for Learning and Memory, Department of Brain and Cognitive Sciences
Massachusetts Institute of Technology, Cambridge, MA 02139, USA
[3]Brain Science Institute, RIKEN, Wako, Saitama 351-0198, Japan
[4]Saitama University Brain Science Institute, Saitama University, Saitama 338-8570, Japan
[5]These authors contributed equally to this work
*Correspondence: mbosch@mit.edu (M.B.), yhayashi@brain.riken.jp (Y.H.)
http://dx.doi.org/10.1016/j.neuron.2014.03.021

SUMMARY

Synapses store information by long-lasting modifications of their structure and molecular composition, but the precise chronology of these changes has not been studied at single-synapse resolution in real time. Here we describe the spatiotemporal reorganization of postsynaptic substructures during long-term potentiation (LTP) at individual dendritic spines. Proteins translocated to the spine in four distinct patterns through three sequential phases. In the initial phase, the actin cytoskeleton was rapidly remodeled while active cofilin was massively transported to the spine. In the stabilization phase, cofilin formed a stable complex with F-actin, was persistently retained at the spine, and consolidated spine expansion. In contrast, the postsynaptic density (PSD) was independently remodeled, as PSD scaffolding proteins did not change their amount and localization until a late protein synthesis-dependent third phase. Our findings show how and when spine substructures are remodeled during LTP and explain why synaptic plasticity rules change over time.

INTRODUCTION

Proteins are distributed into specific subcellular compartments with highly precise spatial and temporal coordination. This is especially crucial for neurons, where the molecular composition of each synaptic connection is independently regulated by its local input activity. This ability of synapses to individually change their structure and composition in a long-lasting way is an essential mechanism for synaptic plasticity and represents the cellular basis of learning and memory.

Most excitatory synapses in the mammalian brain are located on dendritic spines, tiny protrusions arising from the dendrite that act as chemically and electrically segregated microcompartments (Yuste, 2010). Spines are further composed of specialized substructures, such as the postsynaptic density (PSD), a dense matrix of proteins located beneath the synaptic membrane, which serves as a scaffolding platform for glutamate receptors and signaling molecules (Sheng and Hoogenraad, 2007). PSD proteins are, in turn, linked to actin filaments (F-actin), the main structural framework of the spine and a key regulatory site for plasticity (Cingolani and Goda, 2008; Okamoto et al., 2009).

Spines exhibit various forms of structural and functional plasticity. In response to the specific modulation of input activity, the strength of the synaptic transmission can be either long-term potentiated (LTP) or long-term depressed (LTD; Malenka and Bear, 2004). Simultaneously, spines can undergo structural changes, enlarging during LTP and shrinking during LTD (Bosch and Hayashi, 2012). In the CA1 region of the hippocampus, LTP is initiated by the entry of Ca^{2+} through NMDA-type glutamate receptors (NMDARs), which triggers the translocation of specific proteins to the synapse, including AMPA-type glutamate receptors (AMPARs; Hayashi et al., 2000). This early phase of LTP (E-LTP) requires the rapid polymerization of actin and the activation of Ca^{2+}/calmodulin-dependent protein kinase II (CaMKII; Okamoto et al., 2009).

To further consolidate E-LTP into the late phase (L-LTP), the synthesis and transport of new proteins into potentiated synapses are required (Kelleher et al., 2004). But, how can molecules synthesized in the cell body or dendritic shaft specifically identify the potentiated spines from the vast majority of naive spines? Frey and Morris hypothesized that LTP generates a "synaptic tag," responsible for capturing the necessary molecules only into the selected spines (Redondo and Morris, 2011). To date, the molecular identity of this tag and the process of synaptic capture are largely unknown. It is essential, therefore, to identify the molecules that are transported to the spine and the precise time course of this translocation to understand the basic mechanisms of LTP and, thus, of learning and memory.

In this study, we analyzed the evolution of the postsynaptic protein composition during the potentiation of individual spines. We found that multiple proteins were delivered to the synapse in four distinct dynamic patterns and in three sequential temporal

phases. We further studied two intriguing and opposing phenomena: the rapid and persistent accumulation of cofilin and the delayed growth of the PSD. These findings led us to propose a broad mechanistic model for spine reorganization after LTP induction, which explains a number of features associated with synaptic plasticity and metaplasticity and suggests a molecular mechanism for the process of synaptic tagging and capture.

RESULTS

Induction of LTP in Single Dendritic Spines Sequentially Modifies Their Protein Composition

In order to longitudinally visualize the molecular remodeling of the dendritic spine after LTP induction, we selected 15 key postsynaptic proteins that represent different aspects of synapse function: a neurotransmitter receptor (GluA1 subunit of AMPAR), signal transduction molecules (α and β subunits of CaMKII), PSD scaffolding proteins (PSD-95, Homer1b, Shank1b, and SAP97), actin and its regulatory proteins (cofilin-1, actin interacting protein 1 [Aip1], p21 subunit of Arp2/3, and profilin IIA), structural proteins that crosslink F-actin or link it to other structures such as the PSD and the plasma membrane (drebrin A, α-actinin2, and CaMKIIβ), and a dendritic structural protein (septin7). Each of these proteins was fused with a GFP (Table S1 available online) and expressed in CA1 pyramidal cells of rat hippocampal slice cultures, along with a red fluorescent protein (RFP) as a volume marker. GluA1 was fused to superecliptic pHluorin (SEP) and thus represents the amount of receptor inserted into the spine membrane. These fusion proteins have previously been demonstrated to mimic the subcellular localization of endogenous proteins (see references in Table S1). Expression of these proteins did not affect the density or basal size of spines (Figures S1B and S1C).

Consistent with previous reports (Matsuzaki et al., 2004; Harvey and Svoboda, 2007; Steiner et al., 2008; Lee et al., 2009; Govindarajan et al., 2011), induction of LTP in single dendritic spines with two-photon (2P) uncaging of glutamate produced a persistent enlargement of the spine along with a persistent increase of synaptic transmission (Figure S1A). Because of this tight correlation between spine enlargement and AMPAR current potentiation, we subsequently monitored spine structural expansion (structural LTP [sLTP]) as a readout of single-synapse LTP.

Before stimulation, the total amount of protein in the spine head was proportional to the spine volume for all analyzed proteins (Figure S1F), indicating that unstimulated spines have a similar protein composition irrespective of their size, within the same local dendritic segment. Induction of sLTP caused a similar degree of spine expansion among neurons expressing different proteins (Figures S1D and S1E). Concomitantly with spine enlargement, ten of the tested proteins (cofilin, actin, Arp2/3, profilin, drebrin, Aip1, GluA1 [Makino and Malinow, 2009; Patterson et al., 2010], α-actinin, CaMKIIα [Zhang et al., 2008], and CaMKIIβ) efficiently translocated to the spine (Figure 1). In contrast, three other proteins (PSD-95, Homer1b, and Shank1b [Steiner et al., 2008]) did not persistently change their amount for up to 30 min after LTP induction. Interestingly, these three proteins were all scaffolding proteins of the PSD. The amount of SAP97 increased but to a lesser degree than the change in spine volume. Septin7, which was located in the dendritic shaft, remained unaltered.

To compare the time course and the magnitude of accumulation across different proteins, we calculated the relative concentration of each protein in the spine by dividing GFP intensity by RFP intensity (i.e., protein amount divided by spine volume; Figures 2A and 2B). Cofilin showed a rapid increase in concentration starting within the first 20 s after stimulation and was the only protein that remained highly enriched in the spine for up to 30 min. Actin, Aip1, and Arp2/3 initially increased their concentration but eventually returned to their original levels (i.e., the amount of protein scaled proportionally to the change in spine volume). In contrast, profilin, drebrin, GluA1, α-actinin, CaMKIIα, and CaMKIIβ did not follow the initial expansion of the spine and, therefore, transiently reduced their concentration. These proteins subsequently returned to basal concentration at their own specific rate. Free GFP did not change its concentration as it moved in parallel to RFP (Figures S2A and S2E). Combined CaMKIIα+β subunits (as usually found in the synapse) showed an intermediate behavior between α and β subunits expressed alone (Figures S2B, S2C, S2E, and S2F). As SEP-GluA1 detects the amount of the receptor inserted into the surface membrane (Makino and Malinow, 2009; Patterson et al., 2010), we also divided the amount of GluA1 by the estimated spine surface area instead of the spine volume to obtain GluA1 surface density (Figures S2D and S2G). In this case, GluA1 surface density increased during the first minutes and returned close to baseline levels afterward (Figures S2G and S2J). Finally, the amount of the four PSD structural proteins, PSD-95, Homer1b, Shank, and SAP97, remained mostly unchanged and, thus, as the spine volume increased, their concentration in the spine significantly decreased during the subsequent 30 min.

We classified all proteins into four groups according to the pattern of changes in concentration (Figures 2C and S2J): group 1 (G1, those showing a persistent increase), group 2 (G2, those showing a transient increase), group 3 (G3, those showing a transient decrease), and group 4 (G4, those showing a persistent decrease). Additionally, we divided sLTP into two temporal phases (Figures 2A and S2J): an initial remodeling phase (phase I, <7 min), wherein all groups showed a significant change (either an increase or decrease) in spine composition at some point, and a stabilization phase (phase II, >7 min), wherein G2 and G3 proteins recovered their basal concentration, while G1 and G4 proteins remained significantly enriched or depleted, respectively. It is noteworthy that G1 and G2 proteins include actin and actin-modifying factors, G3 includes several actin-stabilizing factors, and G4 is solely composed of PSD scaffolding proteins.

Subspine Protein Redistribution during sLTP

Synaptic proteins are not homogenously distributed within spines but rather segregated in microdomains. To see whether postsynaptic proteins changed their subspine distribution after sLTP, we analyzed representative proteins for each of the four groups in greater spatial detail (Figures 2D–2I). G2 (actin, Arp2/3) and G3 (CaMKIIα, profilin) proteins remained dispersed within the whole spine head at any time before or after sLTP induction (Figures 2E and 2G–2I). In contrast, G4 proteins (Homer1b and PSD-95) remained clustered in the same subspine region while

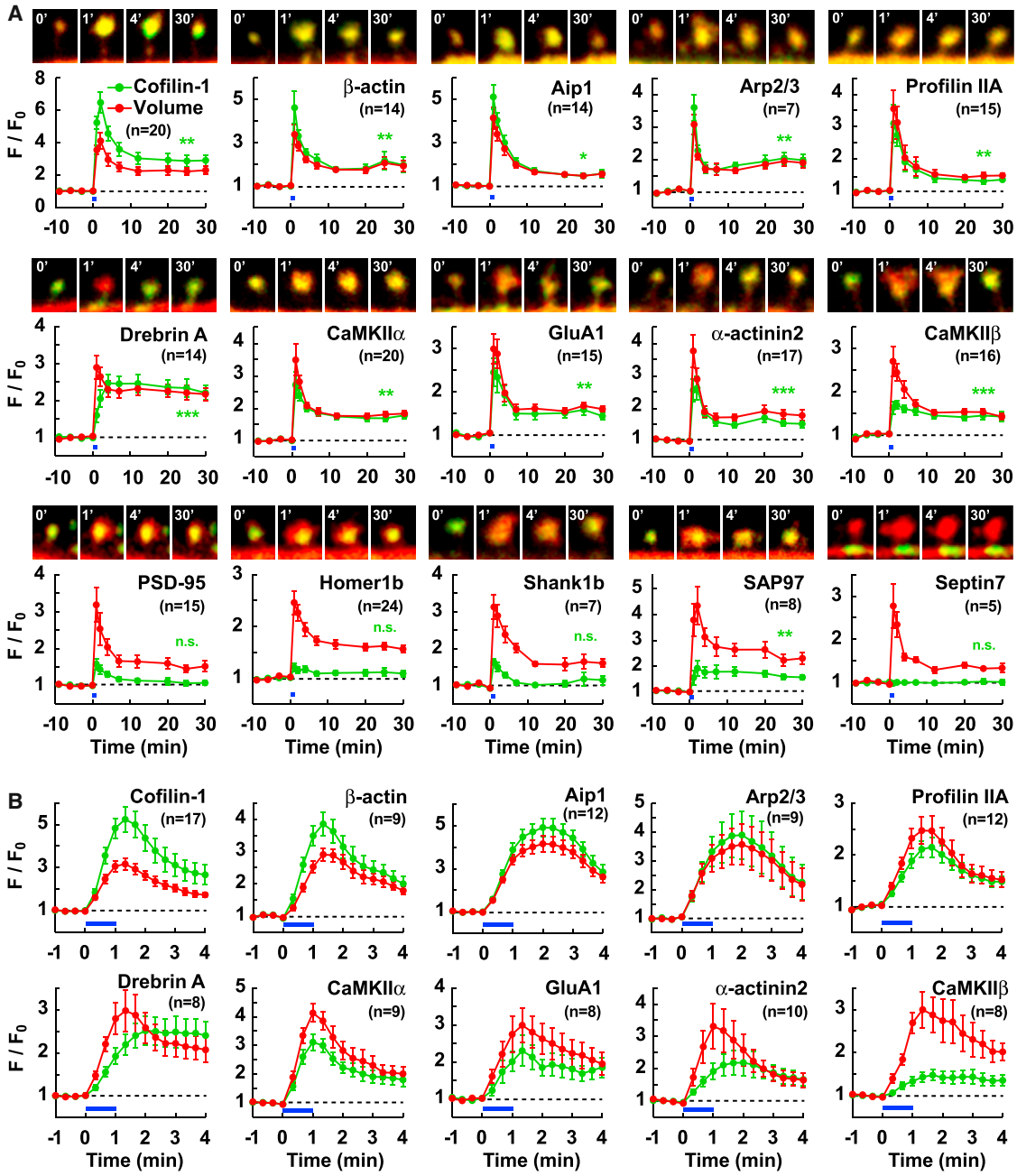

Figure 1. Diverse Temporal Patterns of Postsynaptic Protein Translocation to the Dendritic Spine during sLTP

GFP-tagged proteins were coexpressed with RFP in hippocampal CA1 pyramidal neurons. Single-spine sLTP was induced by 2P glutamate uncaging at 0–1 min (blue bars). Spine volume (RFP, red) and amount of GFP protein in the spine (green) were quantified by measuring the total fluorescence intensity (F) relative to the averaged baseline fluorescence intensity (F_0).

(A) Spine volume and protein amount (mean ± SEM) were monitored for 30 min after sLTP induction. Merged images (3 μm wide; time stamp in min; green, GFP; red, RFP) of representative time-lapse experiments are shown. GluA1 was fused to SEP to detect the spine surface GluA1. Septin7 was measured from the cluster in the dendritic shaft closest to the stimulated spine. *$p < 0.05$, **$p < 0.01$, ***$p < 0.001$: significant differences in protein amount between the 20–30 min interval after sLTP induction and the 10 min baseline (n.s., not significant). Number of experiments is shown in parentheses.

(B) Similar experiments as in (A), at higher temporal resolution (20 s interval) during the first 4 min after sLTP induction, for the ten proteins that showed spine translocation.

See Supplemental Experimental Procedures for statistical analyses. See also Figure S1 and Table S1.

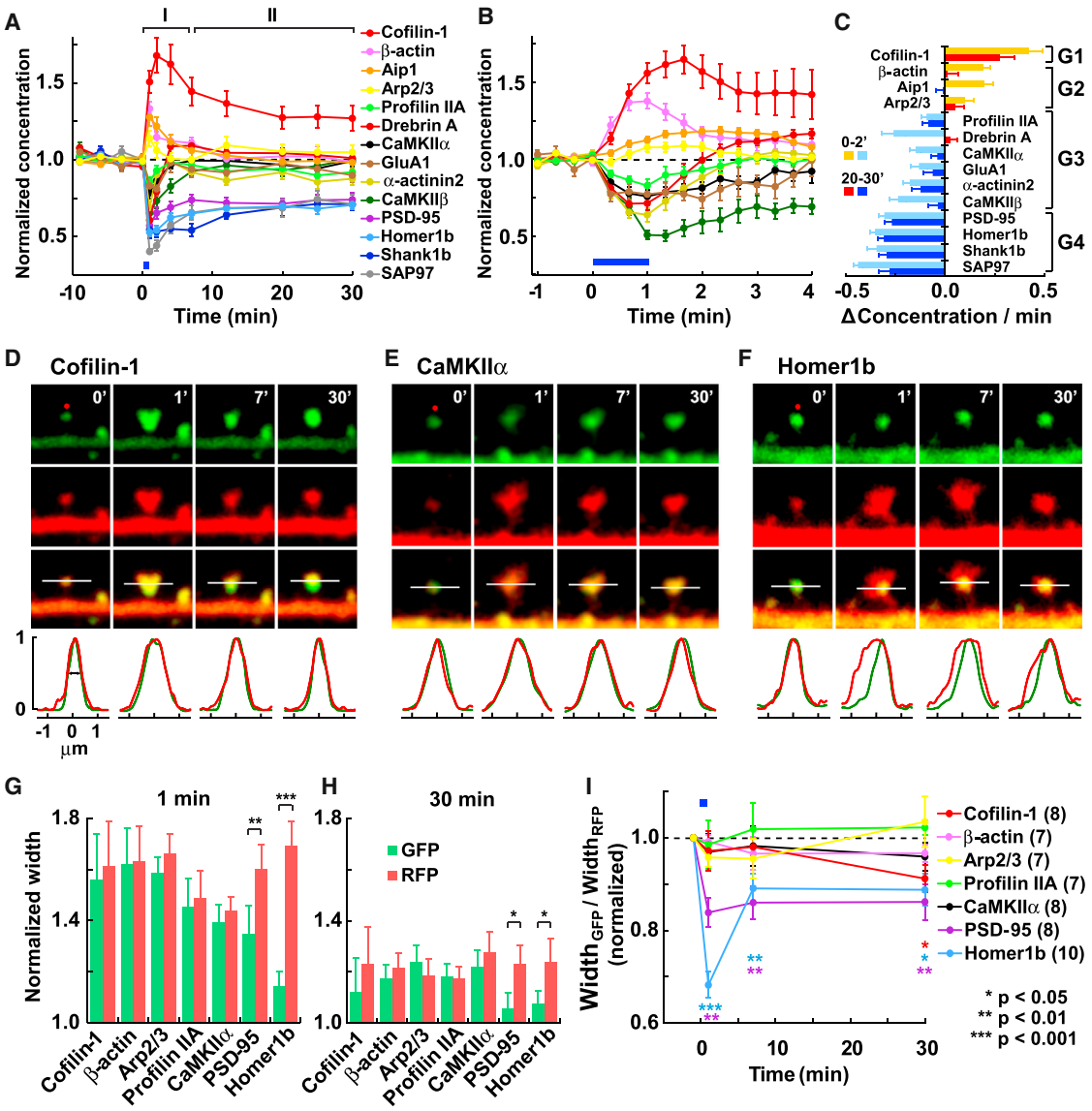

Figure 2. Changes in Spine Concentration and Subspine Distribution of Postsynaptic Proteins during sLTP

(A and B) Relative protein concentration in the spine calculated as the ratio between GFP (protein amount) and RFP (volume) fluorescence intensities (mean ± SEM), normalized to the baseline, during the 30 min (A) or 4 min (B) period after sLTP induction. Data obtained from Figure 1.

(C) Average change in protein concentration per minute during the first 2 min period (0–2′) and the last 10 min period (20–30′). Proteins are classified into four groups (G1–G4) according to the direction (increase or decrease) and persistence (transient or persistent) of the change in concentration after sLTP induction (see text for detail). The transition from phase I to phase II (7 min) was set at the time point where all G2 and G3 proteins were no longer significantly different with respect to the baseline in (A) (detailed statistics in Figure S2J).

(D–F) Spatial distribution of cofilin (D), CaMKIIα (E), and Homer1b (F) within the spine head during sLTP. Green and red fluorescence profiles from a line across the spine head (white line, parallel to the dendrite) were normalized to the peak value. Width was calculated as the full-width at half-height from a Gaussian fitting curve.

(G and H) Averaged green and red widths at 1 min (G) or 30 min (H) after sLTP induction, normalized to baseline levels.

(I) Time course of changes in the relative distribution of the protein within the spine volume (ratio of green width and red width). *p < 0.05, **p < 0.01, ***p < 0.001 with respect to baseline, colored as the corresponding protein. Number of experiments is shown in parentheses. See also Figure S2.

the spine volume increased (Figures 2F–2I). Thus, not only did PSD proteins not change their total amount (Figure 1), but their internal localization was also stably maintained, indicating that they do not contribute to the enlargement of the spine. The G1 protein cofilin existed diffusely in the spine. After sLTP induction, it massively translocated and completely filled the spine head (Figures 2D and 2G–2I). After that, cofilin showed a unique subspine redistribution, with a tendency of gradually accumulating at the center to base subregion of the spine head (Figures S2H and S2I). This phenomenon is further studied in Figures 4A4 and 4A5.

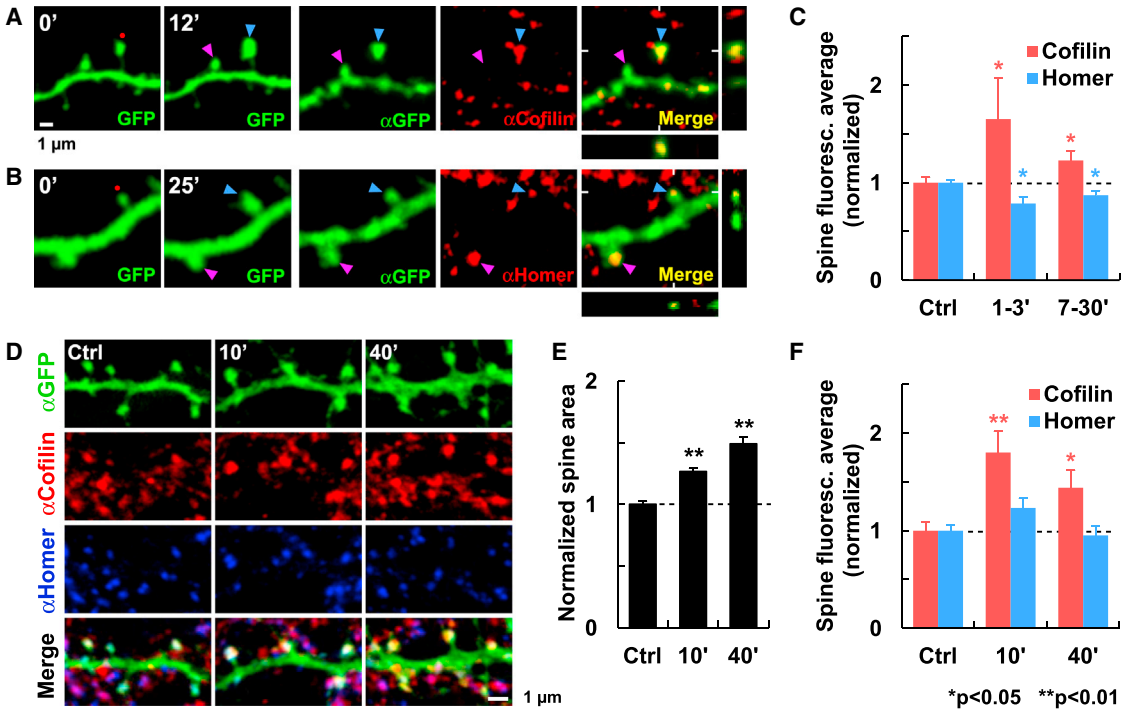

Figure 3. Redistribution of Endogenous Cofilin-1 and Homer1b during sLTP

Subcellular localization of endogenous cofilin-1 and Homer1b were detected by immunohistochemistry after two types of sLTP induction.

(A–C) sLTP was induced in single spines by glutamate uncaging (red dot) in organotypic hippocampal slices. (A and B) Examples of stimulated (blue arrowhead) and unstimulated (pink arrowhead) spines monitored by time-lapse live 2P imaging of GFP up to 12 min (A) or 25 min (B) after sLTP induction. Slices were subsequently fixed and immunostained for GFP (αGFP) and (A) cofilin-1 (αCofilin) or (B) Homer1 (αHomer). XZ and YZ projections are also shown. (C) Quantification of the spine protein concentration measured as the average immunofluorescence (total intensity in the spine head divided by spine area; mean ± SEM) of potentiated spines at two time periods (1–3 min [cofilin, n = 8; Homer, n = 7] or 7–30 min after induction [cofilin, n = 32; Homer, n = 25]) normalized to unstimulated spines (Ctrl; cofilin, n = 85; Homer, n = 118) from the same optical section.

(D–F) Chemical sLTP was induced by application of glycine to dissociated hippocampal cell cultures. (D) Examples of cultures fixed and immunostained for GFP, cofilin-1, and Homer1 before (Ctrl) or at different time points (10 or 40 min) after sLTP induction. (E) Quantification of the increase in spine area normalized to unstimulated spines (n = 38 cells). (F) Quantification of the averaged immunofluorescence in the spine head in potentiated cultures at 10 min (n = 23 cells) or 40 min (n = 20) after stimulation, normalized to unstimulated cultures (Ctrl; n = 22). *p < 0.05, **p < 0.01 with respect to Ctrl. See also Figure S3.

Redistribution of Endogenous Cofilin and Homer1b in the Spine during sLTP

In the above experiments, we studied the dynamics of exogenously expressed GFP-tagged proteins. To rule out the possibility that GFP tagging or overexpression might have altered the natural protein dynamics, we carried out immunohistochemistry to detect the endogenous amounts of two key proteins that showed opposing dynamic behaviors, cofilin and Homer1b. We induced single-spine sLTP by glutamate uncaging in GFP-transfected neurons and fixed the slices at different time points thereafter (Figures 3A–3C). We compared the levels of immunostained signal in potentiated spines with those in surrounding spines in the same optical section. Consistent with our results with GFP-tagged proteins, we found a significant increase in endogenous cofilin concentration in the spine after sLTP, both at the initial phase I and at the persistent phase II (Figures 3A and 3C). In the same way as GFP-Homer1b, endogenous Homer1b concentration decreased both at phase I and II in potentiated spines (Figures 3B and 3C).

In order to confirm these findings in a different preparation, we induced sLTP chemically by application of glycine in dissociated hippocampal primary neurons (Figures 3D–3F; Fortin et al., 2010). We again observed the persistent increase in cofilin concentration in spines from potentiated cultures compared with unstimulated ones. Homer1b concentration did not increase or decrease, probably because of the lack of an early expansion phase with this protocol. We concluded that endogenous cofilin and Homer1b behaved in a similar way during sLTP as our exogenous tagged proteins. Using immunostaining, we also estimated the expression levels of exogenous GFP fusion proteins over endogenous levels to be 2.2 ± 0.2-fold for cofilin and 7.3 ± 1.0-fold for Homer1b at the soma (Figure S3).

sLTP Persistently Modifies the Turnover Rate of Specific Postsynaptic Proteins

What is the mechanism responsible for the redistribution of G1–G3 proteins at the spine? Proteins exist in equilibrium of influx to and efflux from the spine with a turnover rate unique to each protein (Kuriu et al., 2006; Sharma et al., 2006). GFP fusions allowed us to detect the protein movement as a summation of influx and efflux but did not separate between these two processes. To overcome this limitation, we fused photoactivatable GFP

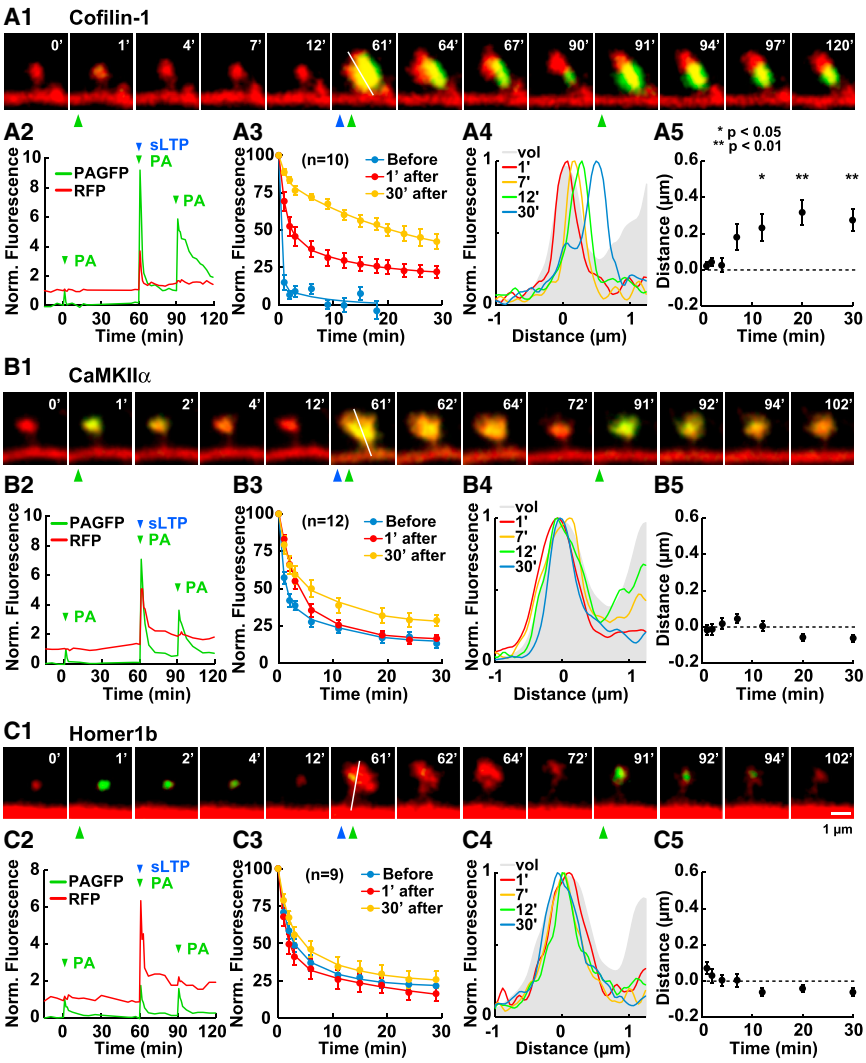

Figure 4. Persistent Changes in Protein Turnover after Single Spine sLTP Induction

The effect of sLTP induction on protein turnover rate was visualized by measuring the fluorescence loss after photoactivation of PAGFP-tagged proteins in the same spine head, before, 1 min, and 30 min after sLTP induction.

(A1) Time-lapse images of a spine from a neuron expressing cofilin-PAGFP. Time of photoactivation (PA) is indicated by green arrowheads and glutamate uncaging (sLTP) by a blue arrowhead.

(A2) Time course of green (normalized to the peak of the first PA) and red (normalized to the initial baseline) fluorescence intensities from the spine head in (A1).

(A3) Averaged fluorescence loss (mean ± SEM) from n (in parentheses) experiments, normalized to the initial peak of each of the three PA time points.

(A4) Fluorescence profiles of cofilin distribution (PAGFP) across a longitudinal axis in the spine head (white line in A1) at different time points after sLTP (normalized to the peak). Profiles are superimposed over the averaged RFP profiles at all time points (vol, gray).

(A5) Average distance between the position of the green and red peaks, indicating how far the stable cofilin cluster is from the center of the spine volume. *$p < 0.05$, **$p < 0.01$ with respect to 1 min after sLTP.

(B1–C5) Similar experiments to (A1–A5), with PAGFP-CaMKIIα (B1–B5) and PAGFP-Homer1b (C1–C5).

(PAGFP; Bloodgood and Sabatini, 2005; Honkura et al., 2008) to cofilin (G1; Figure 4A), CaMKIIα (G3; Figure 4B), and Homer1b (G4; Figure 4C). We then photoactivated the PAGFP-fusion protein in the same single spine at three different time points (before, immediately after, and 30 min after sLTP induction) and estimated the protein efflux rate from the spine by measuring the loss of fluorescence.

CaMKIIα slowed down its turnover immediately after the induction of sLTP (Figures 4B1–4B3). Thirty minutes later, the time constant returned to basal levels but the bound fraction was significantly increased, suggesting the existence of an active mechanism to trap CaMKIIα within the spine, which is consistent with previous studies (Shen et al., 2000; Otmakhov et al., 2004; Zhang et al., 2008). In contrast, Homer1b efflux remained constant before, immediately after, and 30 min after sLTP induction (Figures 4C1–4C3), indicating that Homer1b is at a constant equilibrium of influx and efflux during sLTP. Therefore, the reason why the amount of Homer1b does not change after sLTP induction is not because the protein is immobile.

On the other hand, sLTP induction remarkably changed the turnover of cofilin. Whereas efflux was very fast and no bound fraction was present in the spine before stimulation, sLTP induction immediately slowed down the rate of cofilin efflux from the spine and increased the bound fraction (Figures 4A1–4A3). This effect was even more evident at 30 min after induction. Therefore, the increase in cofilin concentration is due to an increased binding of cofilin to a stable component within the spine. This bound cofilin population was still detectable 60 min after sLTP induction.

The fluorescent signal of freely soluble PAGFP-fused molecules rapidly diffuses away from the spine, thereby allowing us to distinguish the subspine localization of the population of proteins stably bound to the spine from the population of soluble proteins, which was not possible with GFP-tagged molecules or immunostaining. We observed that the stable population of cofilin traveled gradually away from the center of the spine head toward the base of the spine head or the spine neck (Figures 4A4 and 4A5). The average travel speed of this stably bound cofilin across the spine was 19.3 nm/min during the first 12 min and 2.37 nm/min between 12 and 30 min. On the contrary, CaMKIIα and Homer1b did not show such movement after the induction of sLTP (Figures 4B4, 4B5, 4C4, and 4C5).

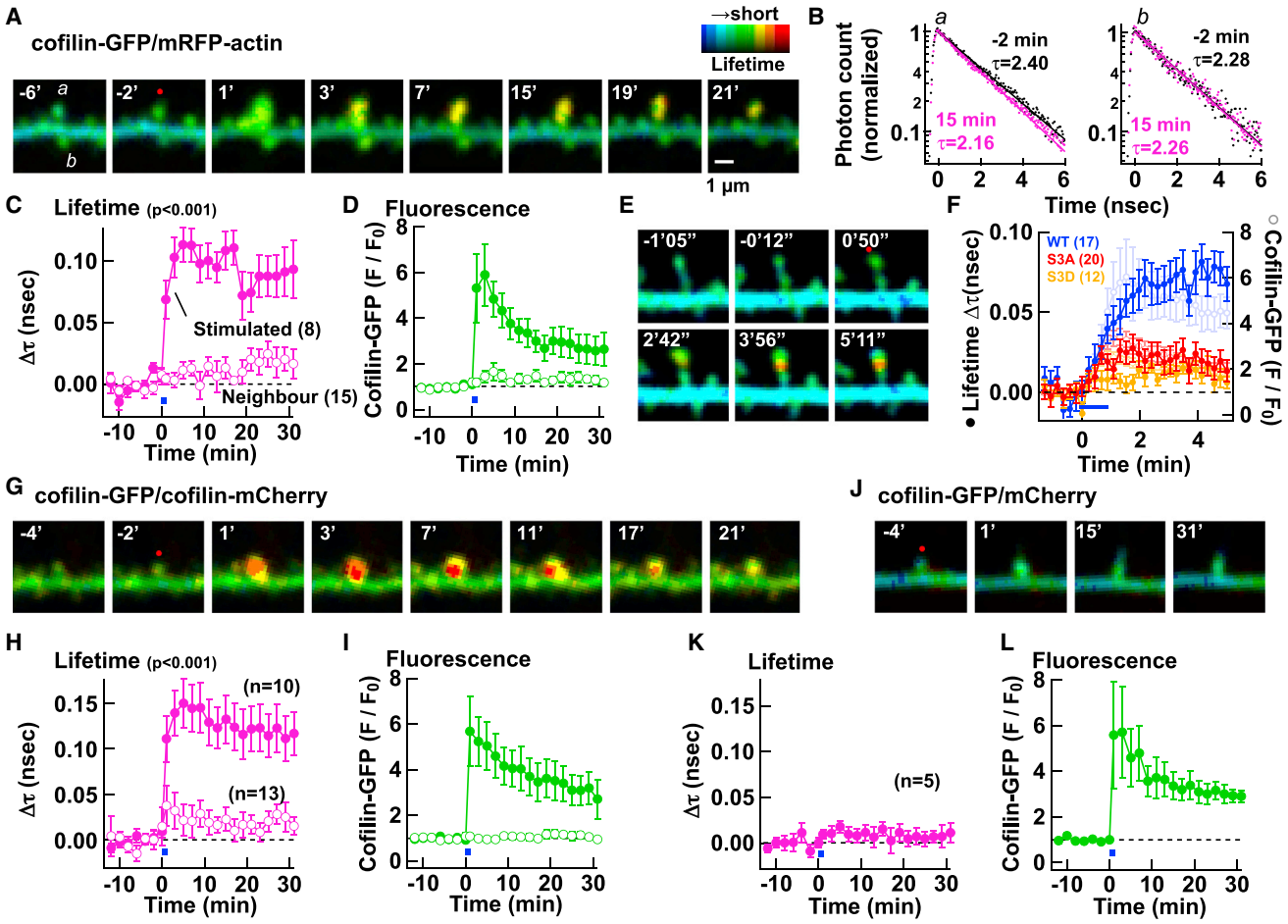

Figure 5. Cofilin Stably Interacts with F-actin at a High Stoichiometric Ratio

(A–F) Interaction between cofilin and actin was monitored by FRET-FLIM between cofilin-GFP and mRFP-actin. (A) Representative time-lapse FLIM images. sLTP was induced in spine *a* (red dot) between 0–1 min. (B) Fluorescence lifetime (τ) of the stimulated spine *a* (left) and an unstimulated spine *b* (right) before (black) and 15 min after sLTP induction (pink). (C and D) Time course of averaged changes in lifetime (C) and amount of cofilin-GFP (D) in stimulated and neighboring spines (mean ± SEM). Number of spines is shown in parentheses. (E) Faster time course images where only one optical section was monitored. (F) Summary of data similar to (E), showing time course of changes in lifetime (filled circles) and amount of cofilin-GFP (open circles) for WT-cofilin, S3A, and S3D cofilin mutants. (G–I) A similar experiment to identify the proximity between cofilin molecules by detecting FRET-FLIM between cofilin-GFP and cofilin-mCherry. (J–L) A negative control experiment with cofilin-GFP and free mCherry. See also Figure S4.

Cofilin Accumulates in the Spine by a Stable Interaction with F-actin

The unique behavior of cofilin prompted us to perform an in depth investigation into the mechanisms of its spine translocation and retention. Considering that cofilin is an actin-binding protein, we reasoned that its retention could be mediated by an increased interaction with F-actin. To visualize the interaction between cofilin and actin, we employed Förster resonance energy transfer-fluorescent lifetime imaging (FRET-FLIM; Lee et al., 2009; Murakoshi et al., 2011) between donor cofilin-GFP and acceptor mRFP-actin (Figures 5A–5F). We confirmed that FRET occurs between cofilin and actin using proteins expressed in heterologous system (Figures S4A and S4B). After sLTP induction, as the amount of cofilin increased and peaked within 1–2 min (Figures 5D and 5F), the FRET signal between cofilin and actin also increased, with some lag, reaching a plateau level in ~3 min, which persisted for up to 30 min (Figures 5C and 5F). In half of the experiments in which only one optical section was monitored in faster scan, we could detect a higher FRET signal at the base of the spine head, consistent with the site of persistent accumulation of cofilin (Figure 5E).

Cofilin has a bidirectional effect on actin polymerization. At a low stoichiometric ratio, cofilin severs F-actin, whereas at a higher ratio, it stabilizes the filaments or even promotes their nucleation and assembly by binding to the long-pitch helix of F-actin (Andrianantoandro and Pollard, 2006). The pitch of actin monomers in the filament is ~55 Å, which is within the optimal detection range for FRET (50–100 Å). We predicted that if cofilin binds F-actin stoichiometrically, cofilin molecules will come close enough to each other to allow FRET. In contrast, if cofilin interacts with F-actin at a low stoichiometric ratio or with G-actin, FRET will not be observed. We validated this interaction in

heterologously expressed proteins in vitro (Figures S4C–S4F). Our results in vivo showed that FRET between cofilin-GFP and cofilin-mCherry persistently increased in the spine after sLTP for at least 30 min (Figures 5G–5I). Spines expressing cofilin-GFP and free mCherry did not show any change in FRET signal (Figures 5J–5L). Together, these results suggest that sLTP induces the formation of a stable cofilin-decorated F-actin complex selectively in the potentiated spine.

sLTP Is Regulated by Cofilin Signaling Pathways

We further investigated the biological significance that cofilin plays in sLTP as well as the signaling pathways that regulate cofilin activity and dynamics (Figure 6). First, to test whether cofilin is required for sLTP, we knocked down cofilin and actin depolymerizing factor (ADF; another protein of the same family), by a combination of specific shRNAs (shCFL and shADF; Endo et al., 2007). We confirmed the efficiency of these shRNAs in dissociated cell cultures (Figures S5A and S5B). When we coexpressed these shRNAs (but not shCFL alone; Figure S5C) together with RFP in slices, we observed a significant reduction in spine enlargement during the persistent phase II (at 20–30 min) of sLTP (Figure 6B). This reduction could be fully rescued by coexpression of shRNA-resistant version of wild-type (WT) cofilin. These results are consistent with a study conducted on cofilin knockout mice, which showed an impairment in electrophysiologically measured LTP (Rust et al., 2010) and demonstrate that cofilin family proteins are necessary for the consolidation of both functional and structural LTP.

One of the major mechanisms to regulate cofilin activity is by phosphorylation at serine (S) 3 (Oser and Condeelis, 2009). We therefore tested whether phosphoblock S3A and phosphomimetic S3D mutants of cofilin (which renders cofilin constitutively active or inactive, respectively) could rescue the effect of shRNA (Figures 6C–6F). S3A mutant was initially enriched in the spine upon sLTP induction but, unlike WT cofilin, it returned to the volume level and was not persistently retained (Figures 6D and 6F). S3D mutant did not show any initial or persistent enrichment, probably because it cannot interact with actin. Consistent with these data, S3A mutant showed an attenuated increase in cofilin:actin FRET signal and S3D did not show any increase in the signal (Figure 5F). Importantly, both mutants failed to rescue the reduction of sLTP by shRNA at 20–30 min (Figures 6C and 6E). Even in the absence of shRNA, where endogenous cofilin is able to sustain a normal sLTP, S3A and S3D mutants showed the same pattern of impaired retention in the spine (Figures S5D–S5G), which demonstrates that this trafficking impairment is due to the mutations and not to the lack of spine enlargement. Taken together, these results indicate that only unphosphorylated cofilin can be initially concentrated at the spine but it needs to be subsequently phosphorylated for long-term retention. We therefore conclude that the consolidation of sLTP into phase II depends on the integrity of the S3 regulatory site of cofilin.

LIM kinase (LIMK) plays the main role of phosphorylating cofilin at S3 (Oser and Condeelis, 2009). We next tested the role of LIMK in sLTP by overexpressing a peptide mimicking the 1–16 amino acids of cofilin, which works as a pseudosubstrate for LIMK (Zhou et al., 2004; Gu et al., 2010; Figures S5J and S5K). We found that this peptide significantly blocked the spine enlargement as well as the translocation of cofilin (Figures 6G, 6O, and 6P). When we knocked down LIMK1 and LIMK2 by shRNA (Endo et al., 2007), we observed a similar reduction in spine enlargement and an impaired persistent retention of cofilin (Figures 6H, 6O, and 6P). LIMK, in turn, is activated by two upstream kinases, p21-activated kinase (PAK) and Rho-associated, coiled-coil containing protein kinase (ROCK), which are downstream of Rac/Cdc42 and Rho small G proteins, respectively (Murakoshi et al., 2011; Figure 6A). The pharmacological inhibition of PAK by IPA-3 (Figures 6I, 6O, and 6P) or inhibition of ROCK by GSK429286 (Figures 6J, 6O, and 6P) both blocked spine enlargement, confirming that the signaling pathway that regulates cofilin through LIMK is important for sLTP.

We further tested whether cofilin trafficking shares similar mechanisms to LTP. The NMDA receptor antagonist AP5 completely abolished both sLTP and cofilin translocation (Figures 6K, 6O, and 6P). Inhibition of the CaMK family with KN93 or KN62 reduced spine enlargement as well as cofilin translocation to a comparable degree (Figures 6L, 6O, and 6P; Figure S5H). In contrast, the mGluR5 antagonist MPEP (Figures 6M, 6O, and 6P) or the phospholipase C (PLC) inhibitor U73122 (Figures 6N, 6O, and 6P) did not block spine enlargement or cofilin translocation. Inhibition of protein synthesis by cycloheximide did not either block spine enlargement or cofilin retention (Figure S5I). Hence, the accumulation of cofilin in the spine showed parallel pharmacological properties to sLTP in that it fully depended on NMDAR activation, partially on the activity of CaMK but not on mGluR, PLC, or synthesis of new proteins (Matsuzaki et al., 2004; Patterson et al., 2010). Altogether, these results demonstrate that, in addition to the known roles of NMDAR and CaMK, the persistent spine enlargement requires cofilin and the temporal regulation of its activity through the PAK/ROCK-LIMK pathways.

Uncoupling between Spine Size and PSD Area after sLTP Revealed by Electron Microscopy

The lack of change in total amount (Figure 1A), subspine distribution (Figures 2F–2I), and turnover rate (Figure 4C) of GFP-tagged PSD scaffolding proteins during the first 30 min after sLTP induction (phases I and II) suggests that the PSD remains structurally unaltered despite the substantial enlargement of the spine. We attempted to confirm this finding by visualizing unlabelled PSD from individually potentiated spines by performing correlated 2P imaging and electron microscopy (EM) together with a specific labeling method that allowed us to relocate the same spine under these two modalities (Figures 7A–7F). We induced sLTP in single spines (Figure 7A), fixed the slice, and drew linear marks pointing to the stimulated spines by photoprecipitation of diaminobenzidine (DAB) with the 2P laser (Tanaka et al., 2005; Figures 7B and 7C). These electrodense landmarks allowed us to unequivocally localize the stimulated spines in the EM images of ultrathin sections (Figure 7D). We then performed 3D reconstructions of the dendrite and spines from serial sections (Figures 7E–7G) and quantified the spine head and neck volumes and the PSD area of unstimulated and stimulated spines at different time points after sLTP induction (Figures 7H–7K).

We found a clear correlation between the spine volume and the area of the PSD in unstimulated spines (Figure 7H),

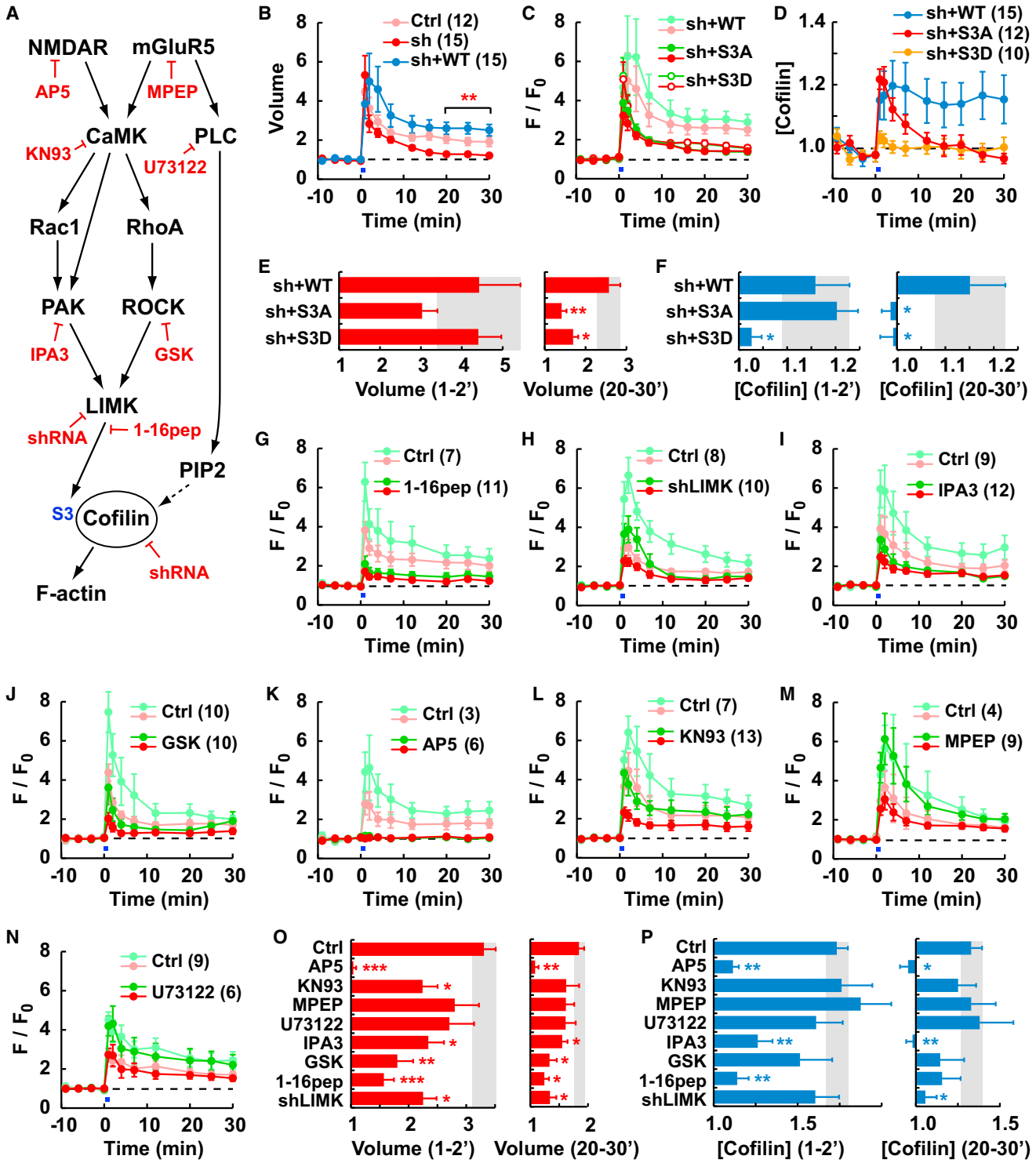

Figure 6. Role of Cofilin in sLTP and Mechanism of Activity-Dependent Translocation and Retention of Cofilin into the Spine

Pharmacological and genetic interventions to study the role that specific elements of the cofilin regulatory pathway play in sLTP and cofilin dynamics.

(A) Schematic diagram of cofilin regulatory pathways showing the pharmacological and genetic tools used (in red).

(B–F) shRNA-mediated knockdown of endogenous cofilin-1 and ADF (shCFL and shADF) and replacement by shRNA-resistant cofilin-GFP mutants. (B) Time course of spine volume (mean ± SEM) after sLTP in the presence of shRNAs (sh), empty shRNA vector (Ctrl), or rescue by WT-cofilin (sh+WT). Number of experiments is shown in parentheses. **p < 0.01 with respect to Ctrl. (C) Time course of spine volume (red lines) and spine amount of cofilin-GFP mutants

(legend continued on next page)

corroborating previous reports (Harris and Stevens, 1989). However, after sLTP induction, this correlation was shifted and stimulated spines showed a deviation from this relationship in that the PSD area was smaller than expected from the volume of the spine, either at 1–2 min or 7–30 min after the stimulation (Figures 7H and 7I). Together with our 2P imaging results, these observations further confirm that the PSD is structurally uncoupled to the spine enlargement during the first 30 min of sLTP. In addition, we observed an increase in the spine neck width at 1–2 min and 7–30 min after sLTP induction without a significant change in spine neck length (Figures 7J and 7K). By approximating the spine neck shape to a cylinder, we estimate that this alteration decreases electrical resistance of the neck by ~40% during the first minute and by ~65% during the 7–30 min after sLTP induction.

Protein Synthesis-Dependent Growth of the PSD in a Late Phase of sLTP

Under basal conditions, spines of a wide range of sizes showed a clear correlation between spine volume and the amount of PSD proteins (Figure S1F) or the area of the PSD (Figure 7H; Harris and Stevens, 1989). Therefore, it is reasonable to assume that the PSD undergoes some structural modification to match the new spine size at some point after induction of sLTP. To answer this question, we monitored the content of Homer1b and Shank1b, two essential components of the PSD framework (Hayashi et al., 2009), for a longer period of time (up to 150 min after sLTP induction). We found that the amount of Homer1b (Figures 8A–8C) and Shank1b (Figures S6A–S6C) in the spine head did not change during the first 45 min but began to increase ~60 min after sLTP induction and was persistently elevated up to 150 min. We termed this as phase III of sLTP (>60 min). There was a clear correlation between the increment of Homer 1b or Shank1b and the increment of spine volume at this phase in every potentiated spine (Figures 8C and S6C). The slope (S) of the regression line was close to 1 at 90–150 min for Homer1b ($S = 0.96$, $R^2 = 0.905$), indicating that the spines had gained an amount of Homer1b closer to the new volume at phase III than that during phases I and II (the same set of spines at 20–30 min: $S = 0.25$, $R^2 = 0.539$).

This delayed capture of PSD scaffolding proteins at the spine prompted us to investigate whether additional molecular mechanisms similar to those implicated in L-LTP were involved. We first used translation inhibitors to test whether the capture of Homer1b was dependent on the synthesis of new proteins. We found that phase I and the early part of phase II (<30 min) of sLTP were not affected by anisomycin (Figure 8D) or cycloheximide (Figure S6D), but the spine enlargement was clearly reduced at phase III. Importantly, the delayed translocation of Homer1b at phase III was totally blocked by these inhibitors. On the other hand, application of brain-derived neurotrophic factor (BDNF), known to trigger local translation and promote L-LTP (Minichiello, 2009), facilitated the spine enlargement, consistent with a previous report (Tanaka et al., 2008) and, concomitantly, enhanced and accelerated (to phases I and II) the accumulation of Homer1b (Figure 8E). These changes were specific to the potentiated synapse since unstimulated spines did not change their size or protein content.

We further confirmed this finding by immunohistochemistry. Using the same methodology as in Figures 3A–3C, we found that endogenous Homer1b behaved similarly to the GFP-tagged protein. Unlike at earlier points (1–30 min; Figures 3A–3C), we did not find any significant difference in Homer1b concentration at 60–80 min between unstimulated and stimulated spines (Figure S6E), suggesting that Homer1b concentration eventually recovered to basal levels. All together, these results strongly indicate that the PSD undergoes a delayed enlargement after induction of sLTP, specifically in the potentiated spine but asynchronously with respect to the spine enlargement. Interestingly, this process shares several properties with L-LTP.

DISCUSSION

The goal of this study was to visualize in real time how the synapse is reorganized during LTP. We wanted to know which proteins are transported to the spine, when they are transported, and how this transport shapes the rules of synaptic plasticity. To this end, we selected multiple key postsynaptic components and studied their dynamic behavior during single-spine-induced LTP. We combined data from all these proteins to build a holistic model that describes the evolution of spine substructures during LTP, divided temporally into three phases.

Phase I: Reorganization of the Spine Actin Cytoskeleton

Phase I (1–7 min) is characterized by a transient but profound modification of the overall protein composition of the spine (see model in Figure 8F). The amount of actin rapidly increases and, as we previously showed, it starts polymerizing into F-actin as fast as ~20 s after LTP induction (Okamoto et al., 2004). Besides this quantitative increase in F-actin, we found a qualitative switch in the composition of actin-binding proteins (ABPs). During these first minutes, the spine is significantly enriched in G1 and G2 proteins. The major function of these proteins is to largely modify F-actin through severing (cofilin), branching (Arp2/3), or capping (Aip1). At the same time, the concentration of G3 proteins is transiently reduced in the spine. Some of these proteins (drebrin, CaMKIIβ, and α-actinin) are known to stabilize the suprastructure of the actin cytoskeleton by bundling F-actin or linking F-actin to the PSD (Okamoto et al., 2007; Sjöblom et al., 2008). Besides, these proteins compete with cofilin and

(green lines) in the presence of shRNAs. (D) Time course of spine concentration (GFP/RFP) of cofilin mutants in the presence of shRNAs. (E and F) Spine volume (E) and cofilin concentration (F) at the 1–2 min or 20–30 min interval after sLTP. *$p < 0.05$, **$p < 0.01$ with respect to sh+WT.
(G–N) Time course of spine volume (red lines) and spine amount of cofilin-GFP (green lines) under experimental (dark color) or control (faint color) conditions. (G) LIMK inhibitor 1–16 peptide (1–16pep). (H) shRNA-mediated knockdown of LIMK1 and LIMK2 (shLIMK). (I) PAK inhibitor IPA3. (J) ROCK inhibitor GSK429286 (GSK). (K) NMDAR inhibitor AP5. (L) CaMK inhibitor KN93. (M) mGluR5 inhibitor MPEP. (N) PLC inhibitor U73122.
(O and P) Spine volume (O) and cofilin concentration (P) at the 1–2 min or 20–30 min interval after sLTP. *$p < 0.05$, **$p < 0.01$, ***$p < 0.001$ with respect to their respective controls. See also Figure S5.

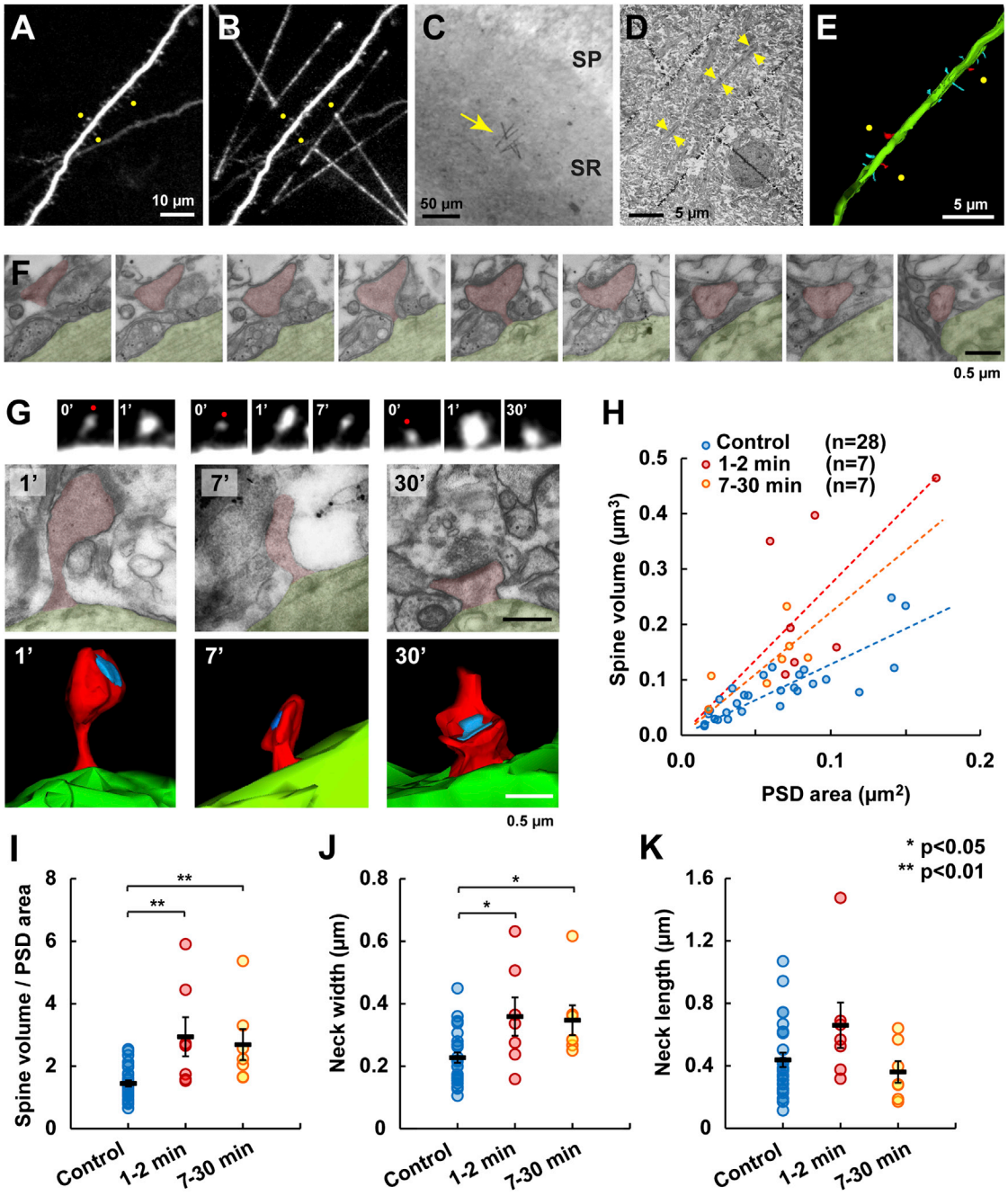

Figure 7. Correlated 2P and EM Imaging Shows that the PSD Remains Unaltered during the Early Phase of sLTP

(A–E) Photo-marking technique to relocalize in EM sections the same spines previously imaged and potentiated with the 2P microscope. (A) Three spines (yellow dots) were stimulated at different time points. (B) 2P laser-induced precipitation of DAB leaves landmarks flanking the dendrite or pointing to the potentiated spines. (C) Landmarks visualized in the hippocampal slice under bright field (arrow). SP, stratum pyramidale; SR, stratum radiatum. (D) Ultrathin EM section showing the same landmarks. Arrows point to the original dendrite. (E) Three-dimensional reconstruction of the same dendrite from serial sections. Potentiated spines colored in red and naive spines in blue.

(F) An example of serial EM images at higher magnification.

(G) Examples of spines potentiated at 1, 7, and 30 min before fixation. Fluorescence time-lapse images, EM images, and three-dimensional reconstructions of the same spines are shown. Blue, PSD; red, spine; green, dendritic shaft.

(H) Correlation between the spine volume and the PSD area in naive control spines and spines at the 1–2 min or 7–30 min interval after sLTP induction.

(I) Same data from (H) plotted as ratio between spine volume and PSD area. Black bars indicate mean ± SEM.

(J and K) Width (J) and length (K) of the reconstructed spine neck.

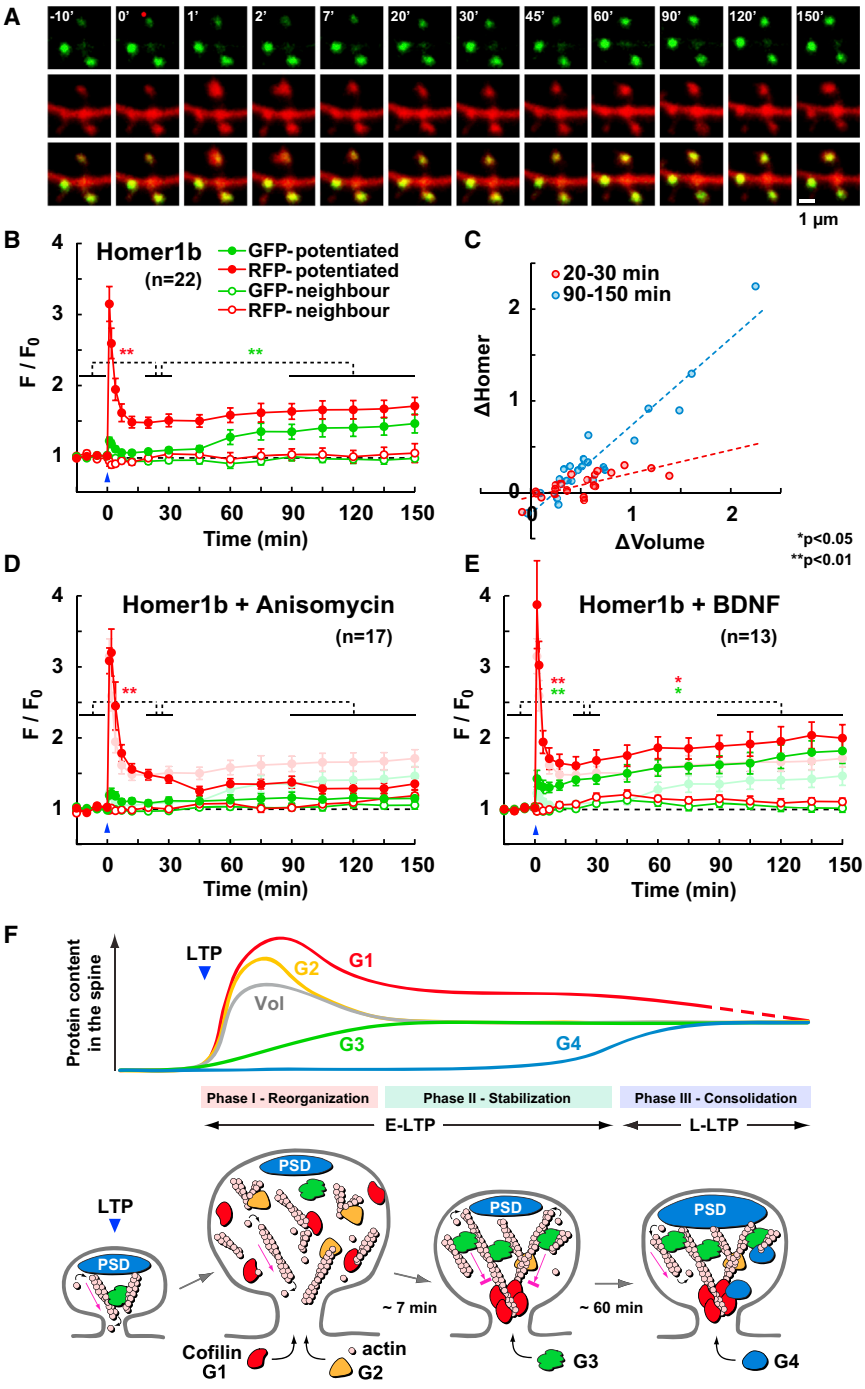

Figure 8. Delayed Synaptic Delivery of Homer1b Shares Properties with L-LTP

Spines expressing Homer1b-GFP were imaged up to 150 min after the induction of sLTP.

(A) Time-lapse images of a potentiated spine (red dot) and two unstimulated spines.

(B) Time course of the amount of GFP-Homer1b in the spine head and the volume of the spine (RFP) after sLTP induction (mean ± SEM).

(C) Correlation between changes in Homer1b amount versus changes in spine volume in the same set of spines at 20–30 min (red) and at 90–150 min (blue) after sLTP induction.

(D and E) Similar experiments but in the presence of anisomycin (D) or BDNF (E). The no-drug data from (B) are shown in faint colors for comparison.

(F) Proposed model for the reorganization of dendritic spine substructures during LTP (see Discussion) based on four patterns of protein dynamics (schematic evolution of the spine amount of G1–G4 proteins; Vol, spine volume) and three temporal phases (I–III). Pink arrow indicates actin treadmilling.

See also Figure S6.

Arp2/3 for F-actin-binding sites (Zhao et al., 2006; K. Kim, personal communication). Therefore, this switch of ABP type from actin-stabilizers to actin-modifiers during phase I generates a time window in which the actin cytoskeleton becomes labile and susceptible to major reorganization.

The fact that cofilin is highly enriched suggests that it might play a major role in this F-actin remodeling. The initial cofilin translocation is triggered by the activation of NMDAR, similarly to functional and structural LTP. Several lines of evidence indicate that cofilin is in its active form during a brief period of time before being inactivated by phosphorylation. First, Aip1 is known to function synergistically with cofilin to cap only free barbed ends of F-actin recently severed by cofilin (Ono, 2003). The increment in Aip1 concentration during the first 1–4 min suggests that cofilin has created those barbed ends during this period. Second, constitutively inactive S3D-cofilin cannot initially translocate to the spine, but constitutively active S3A cofilin does as well as WT-cofilin. And third, Chen et al. (2007) reported that phosphorylation of PAK and cofilin was not detectable until at least 2 min after LTP induction using immunostaining.

What does cofilin do during its transient activation? When the local actin concentration is high, instead of depolymerization, cofilin-severing activity can promote actin polymerization by creating free barbed ends that nucleate new filament growth (Oser and Condeelis, 2009). Because newly formed F-actin is the preferred site for Arp2/3 branching activity (Ichetovkin et al., 2002), Arp2/3 can use those nascent filaments to promote F-actin ramifications. Thus, we postulate that the synergistic action of cofilin and Arp2/3 may create a new set of branched filaments that will be involved in the maintenance of spine expansion and the delivery of new proteins to the synaptic membrane, especially GluA1-containing AMPAR (Shi et al., 2001; Gu et al., 2010). Knocking down cofilin or perturbing its phosphorylation did not

entirely block the initial spine enlargement but did prevent the maintenance of this enlargement. Thus, the remodeling that cofilin and other ABP introduces to the spine cytoarchitecture is necessary for the structural consolidation of the spine in phase II.

Phase II: Stabilization of Newly Remodeled Actin Cytoskeleton and Persistent Accumulation of Cofilin

During phase II (7–60 min), G2 and G3 proteins return to their basal concentration as their amount increases proportionally to the new spine volume. Consequently, the changes introduced in the actin cytoskeleton during phase I can be stabilized to steady-state levels by these new F-actin-stabilizing G3 proteins. Because F-actin is the major direct or indirect binding site for most structural and signaling proteins in the spine, we postulate that the stable increase of F-actin is the primary cause for the spine expansion as well as for the proportional capture of most of the postsynaptic proteins after sLTP (Okamoto et al., 2009). Consistent with this hypothesis, the pharmacological depolymerization of F-actin inhibits the spine enlargement and results in the loss of postsynaptic proteins (Matsuzaki et al., 2004; Kuriu et al., 2006).

In addition, we found a notable qualitative change in the spine during phase II: the persistent accumulation of cofilin at the base of the spine head. Several pieces of evidence indicate that cofilin must be phosphorylated in order to be persistently captured. First, the S3A mutant is initially enriched in the spine but as it cannot be phosphorylated, it is not retained long term. Second, all pharmacological (PAK, ROCK inhibitors) or genetic manipulations (1–16 peptide and shRNA against LIMK1/LIMK2) that prevent cofilin phosphorylation also prevent its persistent accumulation as well as the consolidation of spine enlargement. Third, Chen et al. (2007) showed that PAK and cofilin were phosphorylated within a time window of 2–7 min after LTP induction, which agrees with the transition from phase I to II. And fourth, the upstream signaling molecules Rho and Cdc42 are reported to be activated after induction of sLTP (Murakoshi et al., 2011) and PAK has been found to play an important role in the stabilization of LTP and sLTP (Rex et al., 2009; Murakoshi et al., 2011). Hence, if cofilin is not inactivated in time, the excessive severing activity can reverse the polymerization trend toward depolymerization and thus prevent spine enlargement, as it happens when LIMK activity is reduced (Figure 6), or even induce spine shrinkage, as it happens after induction of LTD (Zhou et al., 2004; Pontrello et al., 2012).

Although p-cofilin cannot bind to actin, we found that cofilin binds to F-actin at a high stoichiometric ratio and forms a new stable structure at the spine core during phase II. To solve this paradox, we speculate that phosphorylation is transient and cofilin is dephosphorylated again before binding F-actin. Indeed, Chen et al. (2007) found that the amount of p-cofilin went back to baseline levels ~7 min after LTP induction. Continuous cycles of cofilin activation/inactivation, tightly regulated in space and time, have been reported in other subcellular structures such as filopodia, lamelipodia, and growth cones when they experience rapid structural changes (Song et al., 2006; Oser and Condeelis, 2009). Therefore, it is no surprise that similar mechanisms take place in dendritic spines.

It is particularly interesting that Honkura et al. (2008) observed the formation of a new stable pool of F-actin ("enlargement pool") specifically in those spines where sLTP was induced. We postulate that this new pool is stabilized by cofilin to form the stable F-actin:cofilin complex that we observed in our study, as they share similar subspine localization, time course, and specificity for potentiated spines. In vitro studies have characterized the properties of this complex, such as F-actin bundling and nucleating activities, which reduces overall actin treadmilling and stabilizes actin filaments (Galkin et al., 2001; Andrianantoandro and Pollard, 2006). What function could this complex have? Recent subspine imaging studies showed that F-actin displays a constant movement from the periphery to the center of the spine through a treadmilling process (Honkura et al., 2008; Frost et al., 2010). LTP induction slows down this movement as the spine expands (Honkura et al., 2008). We propose that the formation of this F-actin:cofilin complex during sLTP is responsible for this phenomenon. Cofilin preferably binds actin in ADP form, rather than ATP or ADP-Pi forms (Oser and Condeelis, 2009), and so it is reasonable that it accumulates at the core of the spine head, where old filaments with a slower rate of turnover exist. The assembly of this complex further slows down the depolymerization and/or the treadmilling rate, providing long-term stability to this F-actin pool. Meanwhile, polymerization can continue at the periphery of the spine head, keeping an outward driving force anchored onto this complex that maintains the structural enlargement of the spine (Figure 8F). In addition to this stabilization role, this complex might exert alternative functions, such as acting as a steric barrier to the diffusion of molecules through the spine neck or acting as a new binding platform to capture extra plasticity-related proteins. We conclude that cofilin is a key bidirectional regulator of spine structural plasticity, as it is implicated in both spine enlargement (this study) and spine shrinkage (Zhou et al., 2004; Pontrello et al., 2012).

Phase III: Delayed Protein Synthesis-Dependent PSD Enlargement during L-LTP

Our 2P imaging (Figures 1, 2, and 4), immunohistochemistry (Figure 3), and EM (Figure 7) experiments confirm that the PSD is structurally unaltered during phases I and II. It actually takes ~60 min before the total spine amount of G4 proteins Homer1b and Shank1b start increasing. This event ultimately defines phase III (Figure 8). The amount of these PSD proteins reached a level that is proportional and closer to the new spine volume, suggesting that the spine eventually recovers the natural correlation between the volume and the PSD size as seen in naive tissue (Harris and Stevens, 1989). Interestingly, the delayed capture of Homer shares several properties with L-LTP. Besides the time course, it is blocked by protein synthesis inhibitors and enhanced by the protein synthesis inducer BDNF. Therefore, we conclude that phases I and II are equivalent to E-LTP and phase III is equivalent to L-LTP at the single-spine level. Hence, L-LTP represents the consolidation into a more mature state of the synapse, where the PSD is structurally remodeled by newly synthesized factors.

It is known that overexpression of some G4 proteins enhances AMPAR-mediated transmission in a way that mimics and occludes LTP (Nakagawa et al., 2004). This led to a proposal that

PSD proteins may constitute "slots" for AMPAR (Shi et al., 2001). Our results do not favor the model that an increase in PSD proteins is responsible for the increase in the number of AMPAR during E-LTP. Instead, our results suggest that empty slot proteins are already present in the PSD and that they display enhanced affinity for AMPAR (e.g., by phosphorylation) to retain them after LTP induction.

Molecular Mechanisms of Metaplasticity, Tagging, and Capture

Our findings provide a reasonable explanation at the molecular level for various known features of plasticity and metaplasticity, including synaptic lability, synaptic saturation, and synaptic tagging.

First, it has been shown that a depotentiation protocol can reverse LTP if applied within a short time window after its induction. As the potentiated state is gradually consolidated, synapses become more difficult to depotentiate (Huang and Hsu, 2001; Yang et al., 2008; Gu et al., 2010). This labile period can be explained by the relative scarcity of G3 actin-stabilizing proteins during phase I, which leaves the remodeled actin cytoskeleton still fragile and able to revert to the previous state. The recovery of protein composition that takes place in phases II and III, when additional G3 and G4 proteins accumulate in the spine, provides a higher level of structural stability, and allows the synaptic consolidation of the potentiated state.

Second, it is known that once a set of synapses receives a strong LTP stimulation, they become saturated, i.e., resistant to further LTP induction. This phenomenon happens during E-LTP and it is not until L-LTP that the same set of synapses can be potentiated again (Frey et al., 1995; Lynch et al., 2013). We propose that the inalterability of the PSD that we observed during E-LTP is responsible for this saturation effect. AMPAR are incorporated into available slots in the PSD after LTP induction. Because the size of the PSD and therefore the number of slots do not increase during E-LTP, once all slots are occupied, the synapse becomes saturated. Only after the arrival of more G4 proteins at the spine during L-LTP and the consequent enlargement of the PSD do new empty slots become available for more AMPAR to be incorporated into the synapse.

Third, the "synapse tagging and capture" hypothesis states that the tag occurs specifically at potentiated synapses, without requiring new protein synthesis, lasting for at least 1–2 hr and, importantly, capable of recruiting newly synthesized plasticity-related products. We propose that the synaptic tag is defined by the increased binding capacity of the actin cytoskeleton in two distinct ways. In a quantitative way, the persistent increase of F-actin in the spine provides the proportional increment of docking sites that will capture the right amount of constituent proteins necessary to maintain the potentiated state (Okamoto et al., 2009). Indeed, it has been shown that the pharmacological disruption of F-actin prevents synapse tagging (Ramachandran and Frey, 2009). In a qualitative way, due to its unique biochemical binding capacities (Galkin et al., 2001), the newly formed F-actin:cofilin complex can act as a tag that sorts and captures novel proteins or mRNAs not present before in the spine. It is ideally located at the base of the spine head, where it can anchor new structures such as the spine apparatus, the endoplasmic reticulum, or the translation machinery. In conclusion, we hypothesize that the main reason for the enlargement of spines might not be to permit functional LTP but, instead, to act as a synaptic tag for the later consolidation of the potentiated state. This view is supported by recent experiments showing the dissociation between functional and structural LTP (Yang et al., 2008; Gu et al., 2010; Redondo and Morris, 2011).

EXPERIMENTAL PROCEDURES

2P Microscopy Imaging and Induction of sLTP in Single Spines

Rat hippocampal organotypic slice cultures were transfected with a plasmid expressing RFP (DsRed2) and a plasmid expressing one of the GFP-fusion proteins (Table S1). Imaging was carried out with a 2P microscope (Olympus) with two Ti:sapphire lasers (Sprectra-Physics) in apical dendrites of CA1 pyramidal neurons (Okamoto et al., 2004). We induced sLTP on small mushroom spines by uncaging MNI-glutamate with 1 ms laser pulses (720 nm) repeated at 1 Hz for 1 min in Mg-free solution (Matsuzaki et al., 2004). GFPs and RFPs were simultaneously excited at 910 nm. PAGFP photoactivation was performed at 820 nm.

Image Analysis

At every time point, a series of seven to ten images were taken every 1 μm of depth and summed (z stacked). A constant region of interest was outlined around the spine head and half of the spine neck and the total integrated fluorescence intensity of the green and the red channels was calculated using ImageJ (by W.S.Rasband, U.S. National Institutes of Health). Values were background subtracted and corrected for bleedthrough and overall fluorescence fluctuations. We assumed that the spine volume and the amount of fusion protein were proportional to the integrated intensity of the RFP and the GFP signal, respectively (Svoboda, 2004). Spine surface area was calculated as the two-thirds power of the volume of a hypothetical sphere (Patterson et al., 2010). For analysis of the distribution of GFP-fused proteins within the spine, a line was drawn across the spine head, centered on the peak of maximum RFP signal, parallel (Figure 2) or semiperpendicular (Figure 4) to the dendrite, and the GFP and RFP intensity profiles were calculated and normalized to their own peak. These profiles were fitted to a Gaussian curve using GraphPad Prism to calculate the full-width at half-maximum.

Fluorescence Lifetime Imaging Microscopy

Fluorescence lifetime was measured using time-correlated photon-counting technology (Becker and Hickl) at 910 nm excitation. Detection was synchronized with excitation light pulse using an external detector. Bleedthrough of the acceptor fluorescence into the emission channel was negligible. A z stack scanned at 0.7 μm separation was summed, except for Figures 5E and 5F, where only a single plane was scanned. Average fluorescence lifetime in the spine head was calculated (Lee et al., 2009; Murakoshi et al., 2011) and presented as the difference from baseline.

Immunostaining after Glutamate Uncaging sLTP

We induced sLTP in spines from GFP-transfected neurons located close to the slice surface. Slices were fixed at different time points in cold 4% paraformaldehyde (PFA) for 15 s, microwaved for 10–15 s, submerged in PFA for 4 min, frozen in liquid N_2 for 15 s, and put back to PFA for 45 min at room temperature. Slices were blocked, permeabilized, and immunostained with anti-cofilin-1 or anti-Homer1 antibodies. Immunofluorescence divided by spine area was blindly measured and normalized to the average image signal and to control spines.

Correlated 2P and EM Imaging

After single spine sLTP induction, slices were fixed with 2% PFA and 2% glutaraldehyde overnight, transferred to the 2P microscope, and perfused continuously with buffer containing diaminobenzidine (DAB) and bubbled with pure oxygen. We localized the same dendritic region and photoprecipitated DAB

by line scanning the tissue with the 720 nm 2P laser (Tanaka et al., 2005). These lines were used as landmarks to correlate 2P and EM images.

See Supplemental Information for fully detailed experimental procedures and statistical analyses.

SUPPLEMENTAL INFORMATION

Supplemental Information includes Supplemental Experimental Procedures, six figures, and one table and can be found with this article online at http://dx.doi.org/10.1016/j.neuron.2014.03.021.

AUTHOR CONTRIBUTIONS

M.B. designed and performed most experiments and wrote the paper. J.C. performed EM. T.S. performed experiments on cofilin knockdown and signaling. H.M. performed electrophysiology and chemical LTP experiments. M.S. supervised the project and contributed to funding. Y.H. designed and supervised the project, performed experiments, contributed to funding, and wrote the paper.

ACKNOWLEDGMENTS

We thank Drs. M.V. Puig, R.K. Narayanan, K. Okamoto, K. Futai, M.K. Hayashi, S. Kwok, A. Govindarajan, I. Israely, S. Tonegawa, B. Bingol, M. Sheng, R. Yasuda, K. Ohashi, K. Mizuno, N. Watanabe, Y. Goda, W. Xu, W. Witke, M. Rust, A. Miyawaki, T. Fukano, C. Yokoyama, and M.F. Bear for sharing resources and helpful discussions; K. Matsuura and L. Avena for technical assistance; and L. Yu for comments on the manuscript. We are grateful to the donors of DNA constructs (Table S1). This work was supported by RIKEN, NIH grant R01DA17310, Grant-in-Aid for Scientific Research (A) and Grant-in-Aid for Scientific Research on Innovative Area "Foundation of Synapse and Neurocircuit Pathology" from the MEXT, Japan, Human Frontier Science Program (Y.H.) and Paul and Anne Punzak Marcus Fund (M.S.). M.B. is a recipient of a "Beatriu de Pinós" fellowship from the "Generalitat de Catalunya" and J.C. of a "Fundación Caja Madrid" fellowship. Y.H. is partly supported by Takeda Pharmaceutical Co. Ltd. and Fujitsu Laboratories.

Accepted: March 6, 2014
Published: April 16, 2014

REFERENCES

Andrianantoandro, E., and Pollard, T.D. (2006). Mechanism of actin filament turnover by severing and nucleation at different concentrations of ADF/cofilin. Mol. Cell *24*, 13–23.

Bloodgood, B.L., and Sabatini, B.L. (2005). Neuronal activity regulates diffusion across the neck of dendritic spines. Science *310*, 866–869.

Bosch, M., and Hayashi, Y. (2012). Structural plasticity of dendritic spines. Curr. Opin. Neurobiol. *22*, 383–388.

Chen, L.Y., Rex, C.S., Casale, M.S., Gall, C.M., and Lynch, G. (2007). Changes in synaptic morphology accompany actin signaling during LTP. J. Neurosci. *27*, 5363–5372.

Cingolani, L.A., and Goda, Y. (2008). Actin in action: the interplay between the actin cytoskeleton and synaptic efficacy. Nat. Rev. Neurosci. *9*, 344–356.

Endo, M., Ohashi, K., and Mizuno, K. (2007). LIM kinase and slingshot are critical for neurite extension. J. Biol. Chem. *282*, 13692–13702.

Fortin, D.A., Davare, M.A., Srivastava, T., Brady, J.D., Nygaard, S., Derkach, V.A., and Soderling, T.R. (2010). Long-term potentiation-dependent spine enlargement requires synaptic Ca^{2+}-permeable AMPA receptors recruited by CaM-kinase I. J. Neurosci. *30*, 11565–11575.

Frey, U., Schollmeier, K., Reymann, K.G., and Seidenbecher, T. (1995). Asymptotic hippocampal long-term potentiation in rats does not preclude additional potentiation at later phases. Neuroscience *67*, 799–807.

Frost, N.A., Shroff, H., Kong, H., Betzig, E., and Blanpied, T.A. (2010). Single-molecule discrimination of discrete perisynaptic and distributed sites of actin filament assembly within dendritic spines. Neuron *67*, 86–99.

Galkin, V.E., Orlova, A., Lukoyanova, N., Wriggers, W., and Egelman, E.H. (2001). Actin depolymerizing factor stabilizes an existing state of F-actin and can change the tilt of F-actin subunits. J. Cell Biol. *153*, 75–86.

Govindarajan, A., Israely, I., Huang, S.Y., and Tonegawa, S. (2011). The dendritic branch is the preferred integrative unit for protein synthesis-dependent LTP. Neuron *69*, 132–146.

Gu, J., Lee, C.W., Fan, Y., Komlos, D., Tang, X., Sun, C., Yu, K., Hartzell, H.C., Chen, G., Bamburg, J.R., and Zheng, J.Q. (2010). ADF/cofilin-mediated actin dynamics regulate AMPA receptor trafficking during synaptic plasticity. Nat. Neurosci. *13*, 1208–1215.

Harris, K.M., and Stevens, J.K. (1989). Dendritic spines of CA 1 pyramidal cells in the rat hippocampus: serial electron microscopy with reference to their biophysical characteristics. J. Neurosci. *9*, 2982–2997.

Harvey, C.D., and Svoboda, K. (2007). Locally dynamic synaptic learning rules in pyramidal neuron dendrites. Nature *450*, 1195–1200.

Hayashi, Y., Shi, S.H., Esteban, J.A., Piccini, A., Poncer, J.C., and Malinow, R. (2000). Driving AMPA receptors into synapses by LTP and CaMKII: requirement for GluR1 and PDZ domain interaction. Science *287*, 2262–2267.

Hayashi, M.K., Tang, C., Verpelli, C., Narayanan, R., Stearns, M.H., Xu, R.M., Li, H., Sala, C., and Hayashi, Y. (2009). The postsynaptic density proteins Homer and Shank form a polymeric network structure. Cell *137*, 159–171.

Honkura, N., Matsuzaki, M., Noguchi, J., Ellis-Davies, G.C., and Kasai, H. (2008). The subspine organization of actin fibers regulates the structure and plasticity of dendritic spines. Neuron *57*, 719–729.

Huang, C.C., and Hsu, K.S. (2001). Progress in understanding the factors regulating reversibility of long-term potentiation. Rev. Neurosci. *12*, 51–68.

Ichetovkin, I., Grant, W., and Condeelis, J. (2002). Cofilin produces newly polymerized actin filaments that are preferred for dendritic nucleation by the Arp2/3 complex. Curr. Biol. *12*, 79–84.

Kelleher, R.J., 3rd, Govindarajan, A., and Tonegawa, S. (2004). Translational regulatory mechanisms in persistent forms of synaptic plasticity. Neuron *44*, 59–73.

Kuriu, T., Inoue, A., Bito, H., Sobue, K., and Okabe, S. (2006). Differential control of postsynaptic density scaffolds via actin-dependent and -independent mechanisms. J. Neurosci. *26*, 7693–7706.

Lee, S.J., Escobedo-Lozoya, Y., Szatmari, E.M., and Yasuda, R. (2009). Activation of CaMKII in single dendritic spines during long-term potentiation. Nature *458*, 299–304.

Lynch, G., Kramár, E.A., Babayan, A.H., Rumbaugh, G., and Gall, C.M. (2013). Differences between synaptic plasticity thresholds result in new timing rules for maximizing long-term potentiation. Neuropharmacology *64*, 27–36.

Makino, H., and Malinow, R. (2009). AMPA receptor incorporation into synapses during LTP: the role of lateral movement and exocytosis. Neuron *64*, 381–390.

Malenka, R.C., and Bear, M.F. (2004). LTP and LTD: an embarrassment of riches. Neuron *44*, 5–21.

Matsuzaki, M., Honkura, N., Ellis-Davies, G.C., and Kasai, H. (2004). Structural basis of long-term potentiation in single dendritic spines. Nature *429*, 761–766.

Minichiello, L. (2009). TrkB signalling pathways in LTP and learning. Nat. Rev. Neurosci. *10*, 850–860.

Murakoshi, H., Wang, H., and Yasuda, R. (2011). Local, persistent activation of Rho GTPases during plasticity of single dendritic spines. Nature *472*, 100–104.

Nakagawa, T., Futai, K., Lashuel, H.A., Lo, I., Okamoto, K., Walz, T., Hayashi, Y., and Sheng, M. (2004). Quaternary structure, protein dynamics, and synaptic function of SAP97 controlled by L27 domain interactions. Neuron *44*, 453–467.

Okamoto, K., Nagai, T., Miyawaki, A., and Hayashi, Y. (2004). Rapid and persistent modulation of actin dynamics regulates postsynaptic reorganization underlying bidirectional plasticity. Nat. Neurosci. *7*, 1104–1112.

Okamoto, K., Narayanan, R., Lee, S.H., Murata, K., and Hayashi, Y. (2007). The role of CaMKII as an F-actin-bundling protein crucial for maintenance of dendritic spine structure. Proc. Natl. Acad. Sci. USA *104*, 6418–6423.

Okamoto, K., Bosch, M., and Hayashi, Y. (2009). The roles of CaMKII and F-actin in the structural plasticity of dendritic spines: a potential molecular identity of a synaptic tag? Physiology (Bethesda) *24*, 357–366.

Ono, S. (2003). Regulation of actin filament dynamics by actin depolymerizing factor/cofilin and actin-interacting protein 1: new blades for twisted filaments. Biochemistry *42*, 13363–13370.

Oser, M., and Condeelis, J. (2009). The cofilin activity cycle in lamellipodia and invadopodia. J. Cell. Biochem. *108*, 1252–1262.

Otmakhov, N., Tao-Cheng, J.H., Carpenter, S., Asrican, B., Dosemeci, A., Reese, T.S., and Lisman, J. (2004). Persistent accumulation of calcium/calmodulin-dependent protein kinase II in dendritic spines after induction of NMDA receptor-dependent chemical long-term potentiation. J. Neurosci. *24*, 9324–9331.

Patterson, M.A., Szatmari, E.M., and Yasuda, R. (2010). AMPA receptors are exocytosed in stimulated spines and adjacent dendrites in a Ras-ERK-dependent manner during long-term potentiation. Proc. Natl. Acad. Sci. USA *107*, 15951–15956.

Pontrello, C.G., Sun, M.Y., Lin, A., Fiacco, T.A., DeFea, K.A., and Ethell, I.M. (2012). Cofilin under control of β-arrestin-2 in NMDA-dependent dendritic spine plasticity, long-term depression (LTD), and learning. Proc. Natl. Acad. Sci. USA *109*, E442–E451.

Ramachandran, B., and Frey, J.U. (2009). Interfering with the actin network and its effect on long-term potentiation and synaptic tagging in hippocampal CA1 neurons in slices in vitro. J. Neurosci. *29*, 12167–12173.

Redondo, R.L., and Morris, R.G. (2011). Making memories last: the synaptic tagging and capture hypothesis. Nat. Rev. Neurosci. *12*, 17–30.

Rex, C.S., Chen, L.Y., Sharma, A., Liu, J., Babayan, A.H., Gall, C.M., and Lynch, G. (2009). Different Rho GTPase-dependent signaling pathways initiate sequential steps in the consolidation of long-term potentiation. J. Cell Biol. *186*, 85–97.

Rust, M.B., Gurniak, C.B., Renner, M., Vara, H., Morando, L., Görlich, A., Sassoè-Pognetto, M., Banchaabouchi, M.A., Giustetto, M., Triller, A., et al. (2010). Learning, AMPA receptor mobility and synaptic plasticity depend on n-cofilin-mediated actin dynamics. EMBO J. *29*, 1889–1902.

Sharma, K., Fong, D.K., and Craig, A.M. (2006). Postsynaptic protein mobility in dendritic spines: long-term regulation by synaptic NMDA receptor activation. Mol. Cell. Neurosci. *31*, 702–712.

Shen, K., Teruel, M.N., Connor, J.H., Shenolikar, S., and Meyer, T. (2000). Molecular memory by reversible translocation of calcium/calmodulin-dependent protein kinase II. Nat. Neurosci. *3*, 881–886.

Sheng, M., and Hoogenraad, C.C. (2007). The postsynaptic architecture of excitatory synapses: a more quantitative view. Annu. Rev. Biochem. *76*, 823–847.

Shi, S.H., Hayashi, Y., Esteban, J.A., and Malinow, R. (2001). Subunit-specific rules governing AMPA receptor trafficking to synapses in hippocampal pyramidal neurons. Cell *105*, 331–343.

Sjöblom, B., Salmazo, A., and Djinović-Carugo, K. (2008). α-actinin structure and regulation. Cell. Mol. Life Sci. *65*, 2688–2701.

Song, X., Chen, X., Yamaguchi, H., Mouneimne, G., Condeelis, J.S., and Eddy, R.J. (2006). Initiation of cofilin activity in response to EGF is uncoupled from cofilin phosphorylation and dephosphorylation in carcinoma cells. J. Cell Sci. *119*, 2871–2881.

Steiner, P., Higley, M.J., Xu, W., Czervionke, B.L., Malenka, R.C., and Sabatini, B.L. (2008). Destabilization of the postsynaptic density by PSD-95 serine 73 phosphorylation inhibits spine growth and synaptic plasticity. Neuron *60*, 788–802.

Svoboda, K. (2004). Do spines and dendrites distribute dye evenly? Trends Neurosci. *27*, 445–446.

Tanaka, J., Matsuzaki, M., Tarusawa, E., Momiyama, A., Molnar, E., Kasai, H., and Shigemoto, R. (2005). Number and density of AMPA receptors in single synapses in immature cerebellum. J. Neurosci. *25*, 799–807.

Tanaka, J., Horiike, Y., Matsuzaki, M., Miyazaki, T., Ellis-Davies, G.C., and Kasai, H. (2008). Protein synthesis and neurotrophin-dependent structural plasticity of single dendritic spines. Science *319*, 1683–1687.

Yang, Y., Wang, X.B., Frerking, M., and Zhou, Q. (2008). Spine expansion and stabilization associated with long-term potentiation. J. Neurosci. *28*, 5740–5751.

Yuste, R. (2010). Dendritic Spines. (Cambridge: The MIT Press).

Zhang, Y.P., Holbro, N., and Oertner, T.G. (2008). Optical induction of plasticity at single synapses reveals input-specific accumulation of alphaCaMKII. Proc. Natl. Acad. Sci. USA *105*, 12039–12044.

Zhao, L., Ma, Q.L., Calon, F., Harris-White, M.E., Yang, F., Lim, G.P., Morihara, T., Ubeda, O.J., Ambegaokar, S., Hansen, J.E., et al. (2006). Role of p21-activated kinase pathway defects in the cognitive deficits of Alzheimer disease. Nat. Neurosci. *9*, 234–242.

Zhou, Q., Homma, K.J., and Poo, M.M. (2004). Shrinkage of dendritic spines associated with long-term depression of hippocampal synapses. Neuron *44*, 749–757.